Direct Dynamics Simulations of Unimolecular Dissociation of 1,2-dioxetane

submitted to

Indian Institute of Science Education and Research Pune
in partial fulfillment of the requirements for the
BS-MS Dual Degree Programme

by

Shreyas Malpathak

Indian Institute of Science Education and Research Pune
Dr. Homi Bhabha Road,
Pashan, Pune 411008, India.

April 2018

Supervisor: Prof. William Hase

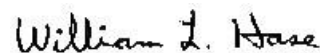Department of Chemistry and Biochemistry

Texas Tech University

Certificate

This is to certify that this dissertation entitled *Direct Dynamics Simulations of Unimolecular Dissociation of 1,2-dioxetane* towards the partial fulfillment of the BS-MS dual degree programme at the Indian Institute of Science Education and Research, Pune represents study/work carried out by Shreyas Malpathak at Texas Tech University under the supervision of Prof. William Hase, Paul Whitfield Horn Professor, Department of Chemistry and Biochemistry during the academic year 2017-18.

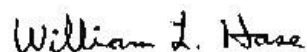Student   Supervisor

Declaration

I hereby declare that the matter embodied in the report entitled *Direct Dynamics Simulations of 1,2-dioxetane Unimolecular Dissociation* are the results of the work carried out by me at the Department of Chemistry and Biochemistry, Texas Tech University, under the supervision of Prof. William Hase and the same has not been submitted elsewhere for any other degree.

Student   Supervisor

Acknowledgements

Undergraduate education at IISER Pune has been a wonderful learning experience and the final year in Lubbock, Texas the cherry on top. I am extremely grateful to Prof. Hase for this unique research opportunity. I am especially thankful to him for allowing me to explore aspects of my project in varied directions; from electronic structure theory to classical chaos, discussions with him were always extremely stimulating.

I am indebted to Dr. Anirban Hazra and Dr. Harinath Chakrapani for the opportunity to work in their research groups, for countless discussions, for encouraging me to explore multiple different aspects of chemistry and for their invaluable advice. Dr. Hazra's Quantum Chemistry and Dr. Chakrapani's Physical Organic Chemistry are to this day my favourite courses at IISER.

Working in a research group has always been a pleasure thanks to many, many wonderful lab-mates. I am especially thankful to Xinyou from Dr. Hase's group who helped me get started in the group and has taught me almost all the programming I know, to Mahesh from Dr. Hazra's group, who taught me how to find transition state structures, and to Ravi, Amogh and Ajay from Dr. Chakrapani's group for attempting to teach me organic synthesis.

Finally, I would like to thank all my friends and family for their constant, unwavering support. Thank you.

Contents

List of Figures

Figure 1: IRC potential energy curve from TSb to $2H_2CO$ dissociation.

Figure 2: Plot of potential energy and $<S^2>$ calculated at UB3LYP/6-31G* and RB3LYP/6-31G*.

Figure 3: A schematic of the motion of a trajectory simulation.

Figure 4: A plot of the total energy and $<S^2>$ versus step number for a trajectory using Algorithms II and III.

Figure 5: Plot of the simulation $\ln[N(t)/N(0)]$ and fit versus time for the A, B, and C excitation groups.

Figure 6: Plot of the simulation $\ln[N(t)/N(0)]$ and fit versus time for the D and random excitation groups and classical harmonic RRKM theory.

Figure 7: Power Spectra for normal modes 1-9 of an undissociated trajectory simulation.

Figure 8: Power Spectra for normal modes 10-18 of an undissociated trajectory simulation.

Figure 9: A schematic of the two-state coupled phase space model.

List of Tables

Table 1: UB3LYP/6-31G* Harmonic Vibrational Frequencies for 1,2-dioxetane.

Table 2: $N(t)/N(0)$ Fitting Parameters for the Simulation Groups.

Table 3: Values for various rate constants obtained from the two-state coupled phase space model.

Abstract

A detailed study of the dynamics of unimolecular dissociation of 1,2-dioxetane (DO) using direct chemical dynamics simulations is presented. Of special interest is the comparison of the dissociation kinetics with the predictions of RRKM theory and implication to the intramolecular vibrational energy redistribution in the molecule. In the process, instabilities observed in unrestricted direct dynamics simulations of homolytic bond dissociation and diradical formation are tackled. A simple and convenient algorithm has been used to circumvent the energy conservation issues related to these instabilities and obtain reliable trajectory simulations. Dissociation probabilities obtained for various initial vibrational excitations are presented and compared with each other and with classical harmonic RRKM theory. DO is found to exhibit intrinsic non-RRKM behavior which is attributed to a) the presence of quasiperiodic trajectories trapped in the phase space ; b) bottlenecks in the IVR between vibrational modes inside and outside the ring.

Chapter 1: Introduction

1,2-dioxetane (DO) has been of interest to chemists since many decades. Early studies focused on synthesis, characterization and decomposition rates of DO and its substituents.[1–7] DO being one of the simplest molecules that exhibits chemiluminescence[8], significant efforts have recently been concentrated into understanding the mechanism behind the chemiluminescence that accompanies the dissociation.[3–5,7,9] Although the precise mechanism is not well established, computational studies opine that the S_1 and T_1 potential energy surfaces, which are very close to the ground state singlet (S_0) surface near the •O-CH$_2$-CH$_2$-O• singlet biradical region (Figure 1), are involved in this mechanism.[7]
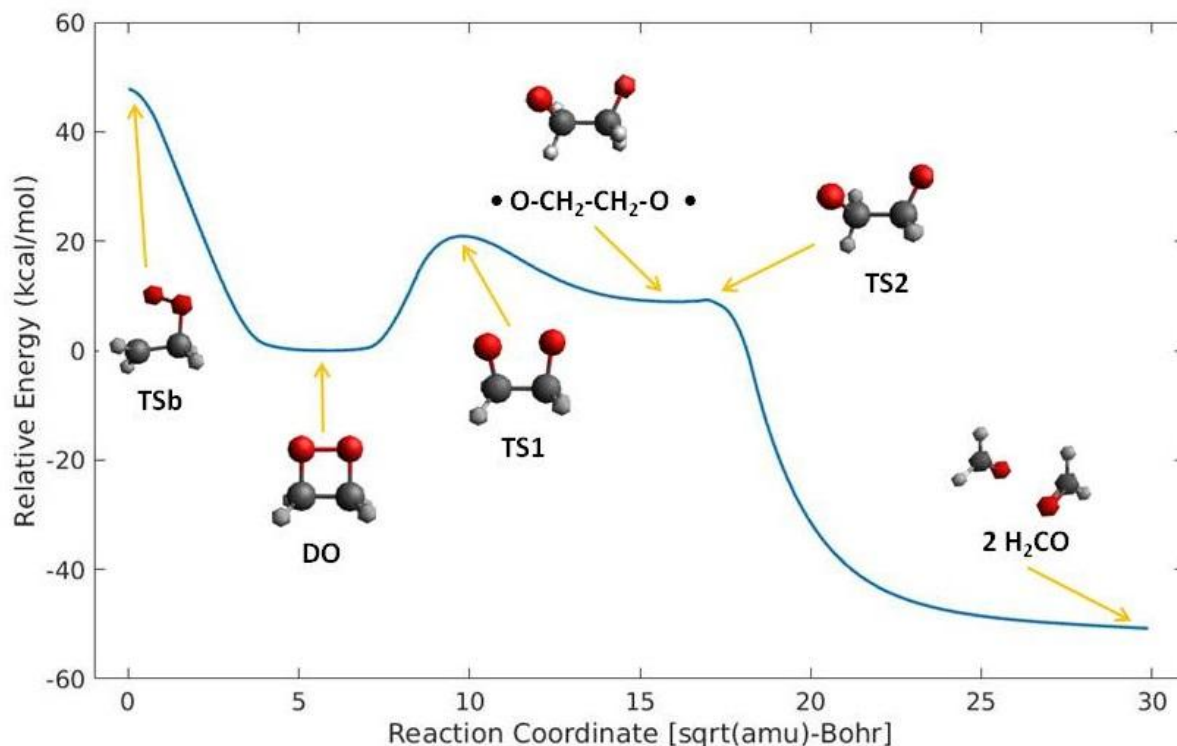
Figure 1: IRC potential energy curve from TSb to 2H$_2$CO dissociation.

Experiments have shown that the chemiluminescence yields for the unimolecular dissociation of DO are less than 0.01[4,10], implying that most of the dissociation might occur completely on the ground state adiabatic singlet PES S_0. Irrespective of which electronic state the product formaldehydes are formed in, the initial reaction from DO to TS1 happens

on the ground state S_0 surface. In spite of the significant interest in the chemiluminescence mechanism, the ground state dissociation has been somewhat neglected. Recent work suggests than DO is formed as an intermediate in the combustion of ethylene with oxygen.[11–16] A detailed study of the dissociation kinetics and dynamics on the ground state would thus certainly be of interest to the combustion and atmospheric chemistry communities.

The bulk of this work is an investigation into the kinetics and dynamics of the dissociation of vibrationally excited DO using direct dynamics simulations.[17] In particular, the dissociation has been compared with the predictions of the Rice-Ramsperger-Kassel-Marcus (RRKM) theory for unimolecular reactions[18] at constant energy. RRKM theory is derived from statistical mechanics with some basic assumptions regarding the structure of the molecule and its phase space. Firstly, RRKM theory assumes that at a fixed total energy all the states of the molecule have an equal probability of being occupied, which results in the reactants forming a microcanonical ensemble. This microcanonical ensemble is assumed to be maintained throughout the reaction. Moreover, in systems that are prepared from non-random excitations (such as chemical excitation), RRKM theory assumes rapid and complete intramolecular vibrational energy redistribution (IVR)[19,20]. In other words, vibrational energy is assumed to be redistributed on a time scale much shorter than the average lifetime of the unimolecular reaction. With this assumption, RRKM theory predicts the following equation for the reaction rate:

$$k_{RRKM}(E) = N^{\ddagger}(E - E_0)/h\,\rho(E) \qquad (1)$$

Here, E is the total energy of the system, $N^{\ddagger}(E)$ is the sum of states for the transition state, E_0 is the potential energy barrier, h is the Planck's constant and $\rho(E)$ is the density of states for the reactant. Although not required for deriving the RRKM rate constant, another approximation that is frequently employed for calculating it is the harmonic approximation which simplifies the calculation of the sum and density of states.[18]

The validity of the predictions of RRKM theory depends on the validity of its assumptions. The harmonic approximation is accurate only near stationary points on the PES and its use may not be appropriate at large energies. Anharmonic corrections to the

sum and density of states, which are required in such cases, may not be easy to calculate. Secondly, and more importantly, the fast IVR assumption needs to be examined more carefully. Studies on van der Waal's[21,22] and ion-molecule complexes in S_N2 reactions[23] have shown weak couplings between intra and intermolecular vibrational modes leading to slow IVR. Identification of any such bottlenecks that may be present in the IVR is intended in this study.

The dynamics of DO dissociation has been investigated using a type of chemical dynamics simulations called direct dynamics.[17] In addition to probing the dynamics, this work also presents a discussion into the subtleties associated with instabilities in direct dynamics using unrestricted electronic structure methods on systems involving homolytic bond cleavage. DO dissociation being one such system, it is essential to address these instabilities to perform reliable simulations.

1.1 Outline

The thesis is divided into chapters that focus on varied aspects of the dissociation dynamics. *Chapter 2* describes the tool used to study the dissociation dynamics, namely direct dynamics simulations. Initial conditions and sampling algorithms implemented in the simulations are discussed towards the beginning of the chapter. The dissociation problem in context of direct dynamics simulations is then presented. The use of a broken-symmetry (BS) guess and its unreliability are highlighted, and a new algorithm is presented, which circumvents the energy conservation problems that arise in such simulations.

Chapter 3 showcases and discusses the results of direct dynamics simulations on the DO system. A comparison of the results obtained for various different groups of trajectories is presented and commented upon. Similarities and differences between groups are highlighted and compared with the predictions of RRKM theory. Power spectra are calculated to verify the existence of quasiperiodic trajectories. A two-state coupled phase model is used to investigate the bottlenecks in IVR. *Chapter 4* concludes.

Chapter 2: Methods

2.1 Direct Dynamics

To probe the dynamics of DO dissociation, this work employs a technique known as direct dynamics, which is a method of simulating chemical reactions using a mix of classical and quantum mechanics. These simulations work under the Born-Oppenheimer (BO) approximation[24] which allows the motion of nuclei to be treated independently from the motion of electrons, enabling the motion of the nuclei to be modeled on an adiabatic potential energy surface (PES) calculated by keeping the nuclei at fixed configurations. Although this approximation works excellently for many systems, care must be taken when multiple energy surfaces are close in energy, in which case the BO approximation breaks down. In this work, the use of direct dynamics implicitly assumes the BO approximation to be valid. Computational studies have shown that the excited state PE surfaces for the dissociation of DO are far apart in energy from the ground state in regions of the PES that are of interest in this study, justifying the use of the BO approximation for these simulations.[7]

In direct dynamics simulations, also known as "on-the-fly" molecular dynamics simulations, the motion of the nuclei on the PES is modeled using classical equations of motion.[17] The potential energy is calculated at each step along the simulation for the required nuclear configuration, eliminating the need to calculate a comprehensive PES. This allows the use of *ab-initio* or density functional electronic structure methods to obtain the potential energy. A typical direct dynamics trajectory may contain as many as 20-30,000 electronic structure calculations, which limits the use of high-level electronic structure methods like CCSD. This drawback can be overcome by performing single-point calculations with high-level electronic structure methods and choosing a lower-level method that predicts similar energies and geometrical parameters, thus ensuring reliability.

The motivation behind investigating the dynamics of DO dissociation is a computational study on the addition of singlet oxygen to ethylene.[16] Direct dynamics simulations were performed at various temperatures starting at TSb (Figure 1), which connects DO to the •O-O-CH_2-CH_2• singlet biradical. These simulations found non-RRKM dynamics characterized by bi-exponential plots of $N(t)/N(0)$ versus time, which prompts the need for a more thorough investigation.

2.2 Description of Trajectory Simulations

To probe DO dissociation dynamics, direct dynamics trajectory simulations were performed with the UB3LYP/6-31G* level of theory, which was also used in the previous study. To understand the effect of non-random excitations on the dynamics, the vibrational modes of DO were divided into four categories depending on their characteristic motions. The DO harmonic vibrational frequencies were calculated at the UB3LYP/6-31G* level of theory using the NWChem electronic structure program.[25] The characteristic motions of the various categories have been presented in Table 1. Group A, B, C and D consist of C—H stretch modes, H—C—H wag and bend modes, out-of-plane motions and ring bend and stretches respectively. A vibrational excitation of 101.6 kcal/mol, including a zero-point energy (ZPE) of 39.06 kcal/mol, was added to each of these groups using quasi-classical sampling.[26] This energy is equivalent to the average energy of the simulations carried out at 1000K in the previous study. In these vibrational excitations, ZPE was added to each mode and the rest of the energy was distributed equally amongst all the modes corresponding to that group. Apart from these four non-random excitations, a fifth group of trajectories were simulated to have random initial conditions using classical microcanonical sampling.[26,27] For all groups no rotational energy was added.

The trajectory simulations were performed using UB3LYP/6-31G* with the VENUS/NWChem chemical dynamics program[28,29] which has algorithms for selecting initial conditions built into it. The trajectories were integrated with a time step of 0.3 fs for a maximum time of 13.5 ps using the velocity-Verlet[30] algorithm. The transition state TS1 has an O—O bond length of 2.1 Å[16], which was fixed as the criterion for dissociation and the

time required to do so was recorded. Recrossing was checked by integrating the trajectories up to an O—O bond length of 2.2 Å; none was observed. The classical harmonic RRKM rate constant was calculated to be 0.64 ps^{-1}. For groups A, B, C and D, 100 trajectories were calculated, whereas for the random excitation group, 200 trajectories were calculated to study the long-time details of the dissociation.

Table 1: UB3LYP/6-31G* Harmonic Vibrational Frequencies for DO.

Mode	Symmetry	Frequency[a]	Description	Group[b]
1	A	111	O-C-C-O torsion	C
2	B	758	Ring bend	D
3	B	867	Ring bend	D
4	A	893	Asym O-O & C-C stretch	D
5	B	944	Asym C-O stretch	D
6	A	1029	Sym O-O & C-C stretch	D
7	A	1078	Sym C-O stretch	D
8	A	1130	Asym H-C-H twist	C
9	B	1175	Sym H-C-H twist	C
10	A	1221	Asym H-C-H rock	C
11	B	1330	Asym H-C-H wag	B
12	A	1383	Sym H-C-H wag	B
13	B	1540	Asym H-C-H bend	B
14	A	1563	Sym H-C-H bend	B
15	B	3047	C-H stretch	A
16	A	3052	C-H stretch	A
17	A	3100	C-H stretch	A
18	B	3117	C-H stretch	A

a. Frequencies in cm^{-1}.

b. Identification of modes for the different simulations groups.

2.3 The Dissociation Problem

The problem of addressing homolytic bond cleavage using electronic structure theory is not new to quantum chemists. It has been described in great detail and lucidity in many quantum chemistry texts.[31,32] At the heart of the problem is the use of unrestricted electronic structure methods to obtain better approximations to the energy and wavefunction of the system. In this work, the dissociation problem has been addressed in context of direct dynamics simulations using unrestricted electronic structure methods. Central to the problem is obtaining potential energies on the correct PES at each step in the direct dynamics simulation, as discussed below.

## 2.3.1 1,2-dioxetane Dissociation Potential Energy Surface

The dissociation problem encountered in the direct dynamics of DO dissociation will be discussed in the upcoming sections. Although calculations have only been performed on this system, the arguments presented hold true for any system involving formation of a diradical due to homolytic bond cleavage.

To understand the problem of interest, a look at the PES surface for the dissociation process is essential. In this work, the PE was calculated using the UB3LYP/6-31G* level of theory. The intrinsic reaction coordinate (IRC) for this unimolecular dissociation involves the formation of the $\bullet O\text{-}CH_2\text{-}CH_2\text{-}O\bullet$ singlet diradical (Figure 1). The two transition states (TS1 and TS2) joining the DO minimum and the products to this diradical both have partial diradical character.

The peculiarities of the direct dynamics of this system, which will be presented in the upcoming sections arise due to the following properties of the PES: a) The reactant region of the PES, near the DO minimum is closed-shell in nature; b) the region near the transition states and the diradical minimum is open-shell in nature; c) the region near the products is closed-shell in nature. A simulation trajectory started near the DO minimum

traverses from a region of closed-shell character into a region of open-shell character, which is crucial to the dissociation problem.

The presence of a homolytic bond cleavage in the system necessitates the use of the unrestricted electronic structure formalism which allows alpha and beta spin electrons to have different spatial wavefunctions.[31,32] This increased variational freedom comes at a small price: unrestricted wavefunctions are not eigenfunction of the S^2 operator. For a singlet diradical, the wavefunction is known to be a linear combination of a singlet and a triplet with equal weights[33,34], resulting in $<S^2> = 1$, and not 0 like that of a true closed-shell singlet. Furthermore, $<S^2>$ rises continuously from 0 for a closed-shell system to 1 for a diradical. Intermediate configurations are known to have $<S^2>$ between 0 and 1. This property can be used to monitor the diradical character of the system.[34] To elaborate further, $<S^2>$ is 0 near the DO minimum and it starts rising as the diradical character of the system increases; $<S^2>$ is 0.76 for TS1 and increases to 1 for the singlet diradical •O-CH_2-CH_2-O•.
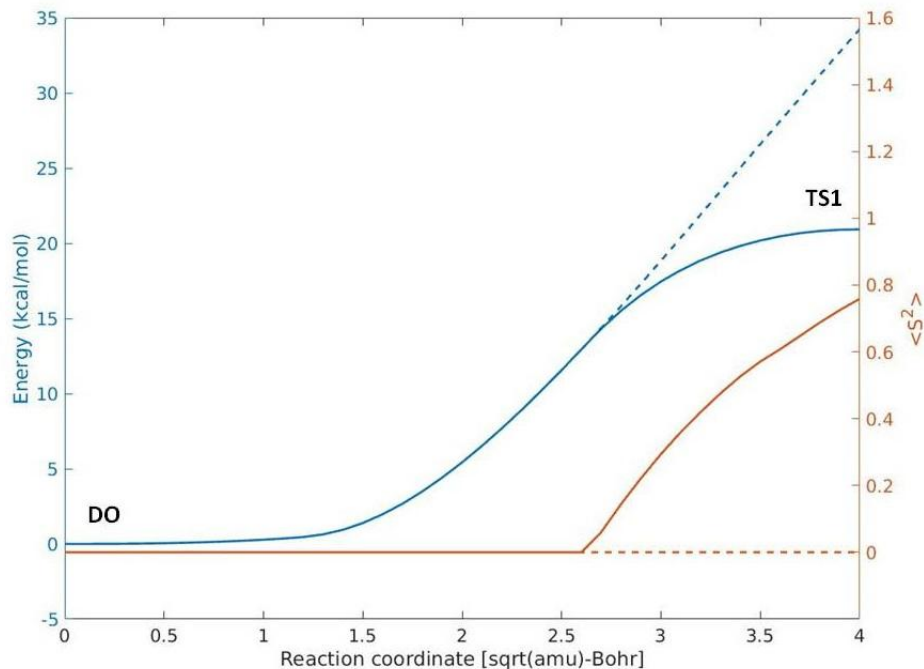
Figure 2: Plot of potential energy (blue) and $<S^2>$ (orange) calculated at UB3LYP/6-31G* (solid line) and RB3LYP/6-31G* (dashed line).

The importance of using the unrestricted formalism is illustrated in Figure 2. In the regions of the PES with significant diradical character, the unrestricted method (UB3LYP) predicts lower energies than the restricted method (RB3LYP). It must also be noted that the onset of the region in which these methods predict different energies is marked by the onset of non-zero $<S^2>$ for the unrestricted method.

2.3.2 The Broken-Symmetry Guess

One of the most important aspects of an unrestricted electronic structure calculation is the guess used for the initial density-matrix. If an unrestricted guess is not provided, the SCF is known to converge to the restricted solution.[31,32] In single point calculations, such an unrestricted guess, also known as a broken-symmetry (BS) guess, is obtained by mixing the HOMO and LUMO orbitals asymmetrically for the alpha and beta spin electrons.[31]

In direct dynamics simulations, the wavefunctions for consecutive steps are expected to be very similar due to extremely small time steps. Taking advantage of this, the wavefunction obtained in the previous step is generally used as the guess for the current step[29] [Algorithm I]. In simulations involving homolytic bond cleavage, such as the system in question, the strategy mentioned above may not be ideal. To obtain an unrestricted solution in open-shell regions, a BS guess is essential. In the region of the potential energy surface where the system transitions from closed shell to open shell, the wavefunction from the previous step which is used as the guess might be restricted, resulting in a restricted solution for the current step. The trajectory will thus continue to traverse on the restricted PES (Figure 3).

One possible way to ensure that a BS guess is used at each step in a direct dynamics simulation is to supply an external BS guess at each step. Such a guess can be obtained by performing a single-point calculation on an appropriate molecular geometry. This modification was implemented in the direct dynamics code as follows [Algorithm II]:
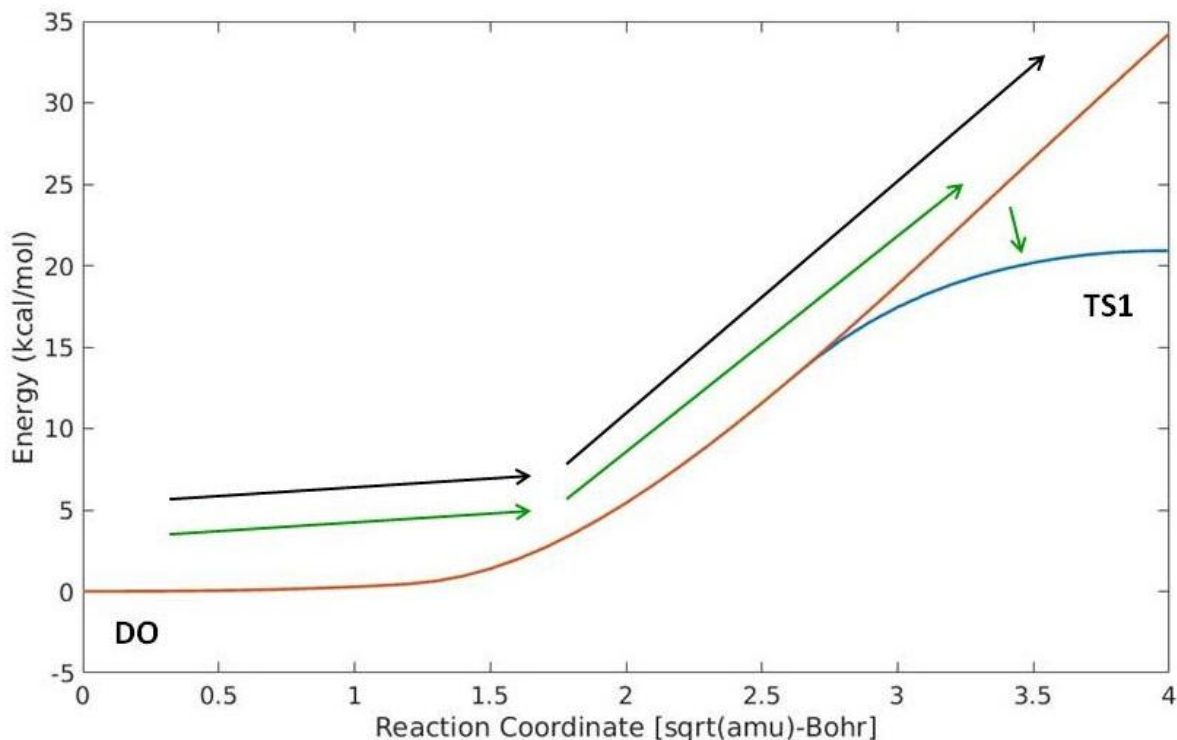
Figure 3: A schematic of the motion of a trajectory. The black and green arrows represent the motion of the trajectories calculated using Algorithm I and II respectively. The orange and blue lines represent the RB3LYP and UB3LYP potential energy curves respectively.

1) The $<S^2>$ is checked at every step in the trajectory. If $<S^2>$ for the previous step wavefunction is less than 0.001, an external BS guess is used.

2) If $<S^2>$ for the previous step wavefunction is more than or equal to 0.001, this wavefunction is used as the BS guess.

Algorithm II ensures that a BS guess is used at each step, which would, at first glance, make it a good candidate for running reliable trajectories. Unfortunately, trajectory simulations suggest otherwise. Plots of total energy and $<S^2>$ versus step number show peculiar jumps. (Figure 4a)
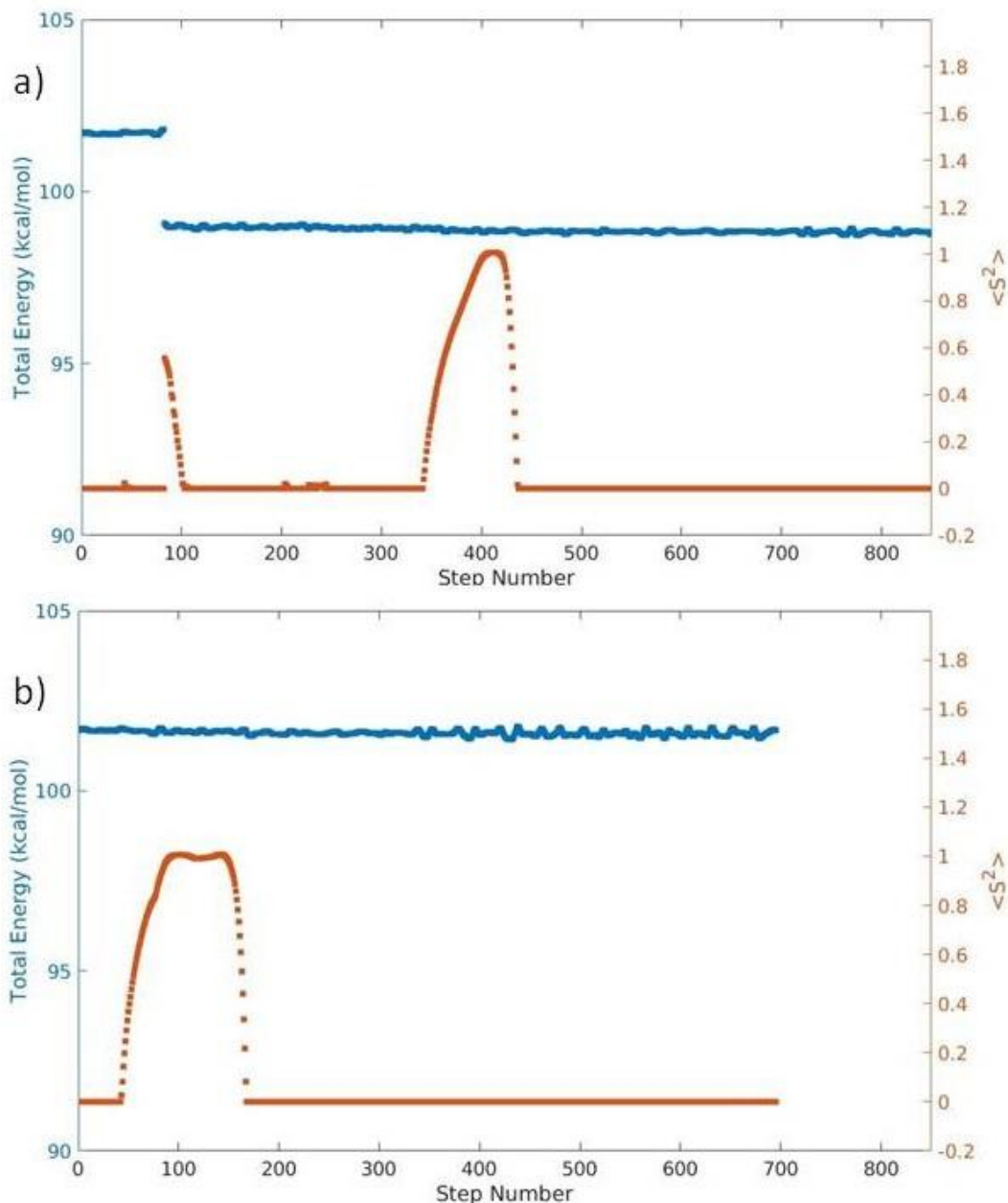
Figure 4: A plot of the total energy (blue) and $<S^2>$ (orange) versus step number for a representative direct dynamics trajectory calculated using a) Algorithm II, b) Algorithm III.

To explain the jumps in total energy and $<S^2>$ a hypothesis has been proposed which relies upon previous work that highlights the unreliable nature of a BS guess: it is necessary to obtain an unrestricted solution, but not sufficient.[35,36] The hypothesis thus

assumes that the SCF procedure may converge to a restricted solution in spite of a BS guess being used. Consider the following scenario: A trajectory runs smoothly on the closed-shell region of the PES. In the region where the system transitions from closed shell to open shell character, an external BS guess is used, which incidentally, fails to obtain the unrestricted solution. A restricted solution is obtained ($<S^2> = 0$) which prompts the external BS guess to be used for the next step. This cycle repeats and the trajectory traverses on the restricted PES, until the SCF converges to the unrestricted solution at a later step. At this point the trajectory jumps from the restricted PES to the unrestricted PES, which is lower in potential energy. As a result, some potential energy is lost, which is seen as the loss in total energy. A schematic of this process is shown in Figure 3. Another aspect which is consistent with this hypothesis is the jump in $<S^2>$. Before the jump, when the trajectory is on the restricted PES, $<S^2>$ is 0, whereas it is non-zero on the unrestricted surface, which is seen as a jump in the $<S^2>$.

With insights from this hypothesis, a modification to the direct dynamics algorithm is presented, with the aim of ensuring that trajectory simulations traverse smoothly on the unrestricted PES. The modified algorithm [Algorithm III] is as follows:

1) The simulation is performed identically like Algorithm II with a minor addition: coordinates and momenta of all atoms are saved every 30 steps.

2) When a jump in total energy is observed, the unrestricted wavefunction obtained after the jump is saved.

3) The trajectory is restarted from the last saved coordinates and momenta, with a small modification: the wavefunction from step 2) is used as the external BS guess.

Two key subtleties need to be mentioned about this algorithm. Firstly, the number of steps at which the coordinates and momenta are saved is chosen such that the trajectory is restarted in the closed shell region of the PES. Secondly, the wavefunctions obtained after the jump are used as the BS guess because they are assumed to be a really good guess. The last saved geometry and the geometry during the jump are not expected to be significantly different because the coordinates and momenta are stored at rather short intervals. Figure

4b shows the same trajectory from 4a run with Algorithm III, which now shows smooth energy conservation and gradual, smooth changes in $<S^2>$.

2.3.3. Reflections and Comments

The algorithm presented in the previous section works excellently for the system of interest, which makes it susceptible to be perceived as a full-proof algorithm, which is far from the truth. Although it can be used for other systems of similar nature with minor modifications, the unreliable nature of this algorithm must be understood. The use of wavefunctions obtained after the jump as the BS guess is extremely convenient; unfortunately, it may not always work. As mentioned in the previous section, a BS guess is always unreliable and the SCF can converge to the restricted solution. This algorithm also overlooks a more subtle aspect of the dynamics. Consider the following scenario. If a trajectory has insufficient energy along the reaction coordinate to reach the TS, it may stay on the restricted surface (even in the open-shell regions) and return to the closed shell regions without ever "jumping", only to later traverse correctly on the unrestricted surface. Such trajectories will end up taking slightly longer to dissociate than they should, and it is not possible to identify them with this algorithm.

A better, much more sophisticated way to solve the issues discussed here would be performing triplet stability calculations at every point in the trajectory simulation. These calculations check if the SCF has converged to a minimum by calculating the eigenvalues of the orbital rotation hessian. The computational feasibility of performing such calculations at every step is questionable.

2.4 Power Spectrum

To probe into the quasiperiodic nature[37] of the trajectories that did not dissociate, power spectra[38] have been calculated. A discussion of relevance of quasiperiodic behavior to reaction dynamics has been presented in Section 3.3. An algorithm to calculate a power spectrum from classical trajectory data has been previously reported[39,40] and has been used here. This algorithm calculates the power spectrum by performing a Fourier

transform on the normal mode momentum autocorrelation function. A simple description follows:

1) The Cartesian momenta obtained from the trajectory simulations for each step are converted into normal mode momenta using the eigenvectors of the mass-weighted hessian.

2) The autocorrelation function for each normal mode momentum is calculated as a function of time τ as follows:

$$C_j(\tau) = \left[\sum_{t=1}^{N} P_j(t)\, P_j(t + \tau)\right]/N \qquad\qquad (2)$$

Here, j is the normal mode coordinate index; t is the time step number in the trajectory and P_j is the jth normal mode momentum. The autocorrelation function is calculated at 2000 points at steps of 6 fs. A trapezoidal apodization is used.[39]

3) The Fourier transform (FT) of the autocorrelation function is calculated. The power spectrum is defined as the square of the absolute value of the FT. Here the power spectrum is calculated for frequencies between 0 and 3200 cm^{-1} at steps of 1.6 cm^{-1}.

Chapter 3: Results and Discussion

3.1 Dissociation Probabilities, Time Delays and Anharmonic Corrections

The percentage of trajectories that dissociated was 94%, 84%, 85%, 95% and 91% for groups A, B, C, D and random respectively. Some of these dissociations involved crossing the TSb barrier and not the TS1 barrier. Figures 5 and 6 show the varied nature of the plots of *N(t)/N(0)* for all the groups.
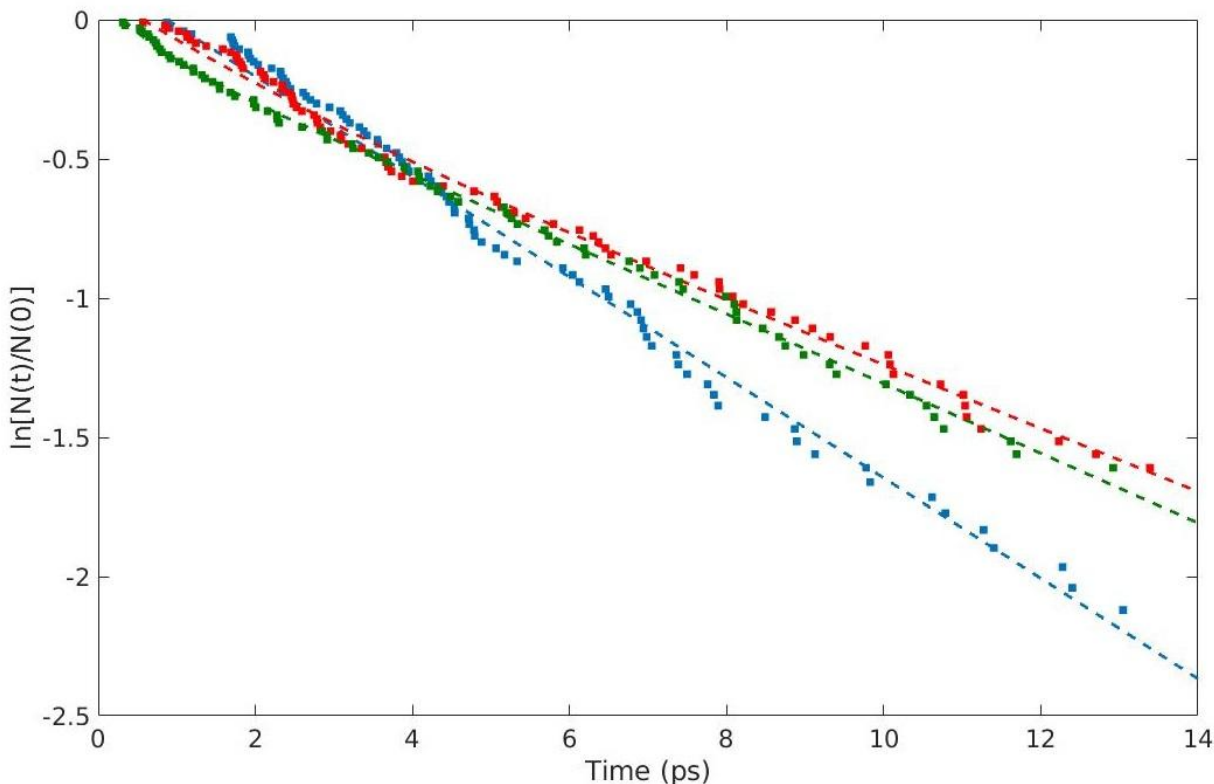
Figure 5: Plot of the simulation $\ln[N(t)/N(0)]$ and fit versus time for the A (blue), B (red), and C (green) excitation groups. Each time a dissociation occurred a point is plotted.

For excitation groups A, B and C, an initial time delay t_0, is observed in the *N(t)/N(0)* plots (Figure 5), whereas no such delay is observed in groups D and random (Figure 6). Table 2 presents precise values.
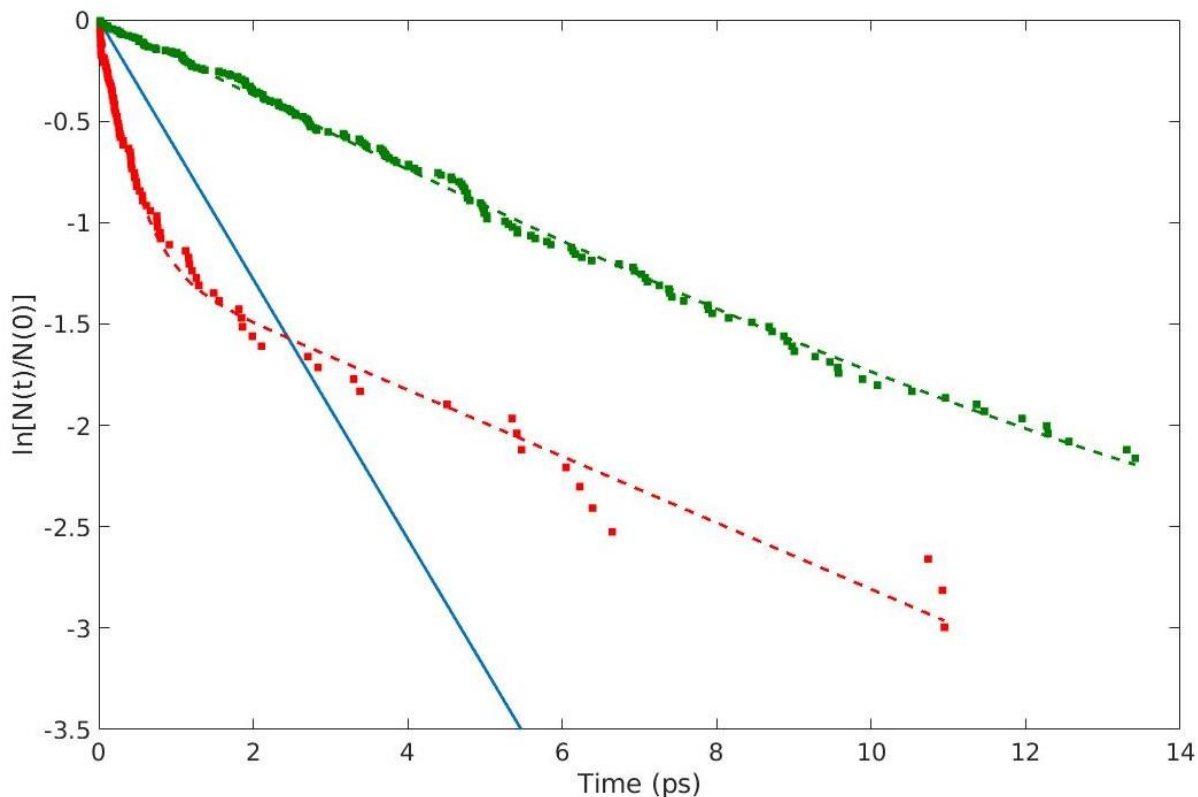
Figure 6: Same as for Figure 5, but for the D (red) and random (green) excitation groups, and for classical harmonic RRKM theory (blue).

For groups A and C an exponential dissociation, shifted by the time delay t_0, is observed:

$$N(t - t_o)/N(0) = \exp\left[-k(t - t_0)\right] \qquad (3)$$

For groups B, D and random, the dissociation is non-exponential, and has been fitted by a bi-exponential function:

$$N(t - t_o)/N(0) = f_1 \exp[-k_1(t - t_0)] + f_2 \exp[-k_2(t - t_0)] \qquad (4)$$

The parameters obtained for these fits are presented in Table 2. Even if a molecule exhibits slow IVR, for an initial microcanonical sampling, a microcanonical ensemble is present at

24

very short times. Thus, for the random group of trajectories, the microcanonical RRKM rate constant can be obtained from the slope of the curve as $t{\to}0$.[41] It can be calculated as follows: $k = [\Delta N/\Delta t]_{t\to 0}/N(0)$. This rate constant for the first five dissociations is calculated as 0.44 ps^{-1}, which is approximately 1.5 times smaller than the classical harmonic RRKM rate constant. The difference in these two rate constants can be attributed to an anharmonic correction.[42–44]

Another aspect of these simulations, which was mentioned earlier, is that a small fraction of the trajectories were found to dissociate via TSb. The percentage of trajectories that dissociated in this manner are 6%, 4%, 5%, 0% and 2% for groups A, B, C, D and random respectively. Compared with the prediction of classical harmonic RRKM theory which stands at 0.6%, these numbers are significantly larger for most of the groups. It must be noted that the anharmonic corrections for the sum of states for the transition states TS1 and TSb are expected to be much smaller than the corrections for the reactant DO, and hence classical RRKM theory should predict correct branching ratios.[44] These results are clearly not in accord with the predictions of RRKM theory.

3.2 Comparison of *N(t)/N(0)* plots

The various different non-random excitation simulations were performed with the intention of being able to compare the results to obtain some insights into the IVR of DO, which will be the focus of this section. Firstly, it must be noted that the reaction coordinate for DO dissociation consists of a substantial component of the O—O stretch. Groups D (ring stretch and bend) and random are expected to have energy initially localized along the reaction coordinate and it is not surprising that the time delay t_0 is ~ 0 for these groups. The time delays observed in group A, B and C simulations are 0.87 ps, 0.24 ps and 0.31 ps respectively, which are significantly larger than the O—O stretch vibrational period, which is ~0.03 ps. These time delays signify the slow IVR from these groups.

Table 2: $N(t)/N(0)$ Fitting Parameters for the Simulation Groups

Group	t_o[a]	f_1	k_1[b]	f_2	k_2[b]
A	0.87	1.00	0.21	0.00	-
B	0.24	0.12	0.18	0.88	0.14
C	0.31	1.00	0.13	0.00	-
D	~0	0.69	3.11	0.31	0.16
Random	~0	0.98	0.20	0.02	~ 0

a. Unit is ps.

b. Unit is ps^{-1}.

For the random excitation group, the $N(t)/N(0)$ is bi-exponential, which makes DO an *intrinsic* non-RRKM molecule[45]. The bi-exponential fit suggests that ~98% of the dissociation occurs with a rate constant (k_1) of 0.20 ps^{-1}, which is approximately half of the anharmonic RRKM rate constant obtained from the short time dissociation. The rest of the dissociation, which follows $k_2 = 1.56 \times 10^{-9}$ ps^{-1}, that is negligible when compared to k_1, is expected to be a manifestation of trapped trajectories with regular/quasiperiodic dynamics[37]. Classical harmonic RRKM theory predicts 0.3% of undissociated trajectories over the 13.5 ps that the trajectories are integrated, whereas the simulations show 9% undissociated trajectories.

Group A and C trajectory simulations interestingly show an exponential dissociation after the initial time delay t_o. In spite of the significant differences in their time delays, both groups show similar rate constants: 0.21 ps^{-1} and 0.13 ps^{-1} for groups A and C respectively. These rate constants are approximately 2-3 times smaller than the anharmonic rate constant.

Group B displays slight bi-exponential behavior after the initial time delay. The rate constants $k_1 = 0.18$ ps^{-1} and $k_2 = 0.14$ps^{-1} obtained from the fit have similar values which are ~3 times smaller than the anharmonic rate constant. Apart from the slight bi-exponential nature, the plots for groups B and C look very similar, which may be explained

by the similarity in their normal mode motions: both groups consist mainly of H—C—H motions.

The results for group D, which comprises of a ring stretches and bends, are the least surprising. The reaction coordinate is closely associated with the modes from group D and thus a very fast initial decay is observed with a rate constant $k_1 = 3.11$ ps^{-1}. Almost 70% of the dissociation is seen to occur at this rate, followed by much slower dissociation with rate constant $k_2 = 0.16$ ps^{-1}, again ~3 times smaller than the anharmonic rate constant.

3.3 Chaotic and Quasiperiodic Motion

Classical mechanical motion can be broadly classified into two categories: chaotic/ergodic and regular/quasiperiodic.[46] RRKM theory assumes complete ergodic behavior of trajectories.[18] At low energies, the vibrational Hamiltonian of a molecular system can be separated into uncoupled harmonic oscillators, which cannot exchange energy and thus exhibit quasiperiodic motion. For higher energies, the harmonic approximation is no longer accurate; anharmonicity and rotational-vibrational couplings can't be ignored.[37] At very high energies, extensive coupling between modes leads to ergodicity. At most energies above the reaction thresholds, both quasiperiodic and chaotic trajectories can exist resulting in *intrinsic* non-RRKM behavior.[47,48]

The bi-exponential fit to the *N(t)/N(0)* plot for the microcanonical random excitation group shows an extremely small long time rate constant k_2. As mentioned earlier, this might be a manifestation of the presence of quasiperiodic trajectories. Such trajectories exhibit little to no coupling between vibrational modes and are thus trapped in phase space – they are very unlikely to dissociate. The presence of such quasiperiodic trajectories can be investigated by calculating the power spectrum of a dynamic variable of the trajectories that do not dissociate. A power spectrum of quasiperiodic trajectories shows sharp peaks in contrast to the broad peaks of chaotic trajectories.[46] Figures 7 and 8 show the power spectrum for one representative trajectory. The sharp peaks seen in the power spectrum are telling of the quasiperiodic nature.

Figure 7: Power Spectra for several normal modes (Table 1) of a representative trajectory from the random group that did not dissociate. The x-axis is frequency from 0 to 3200 cm^{-1} and the y-axis is energy/cm^{-1} (arbitrary units).
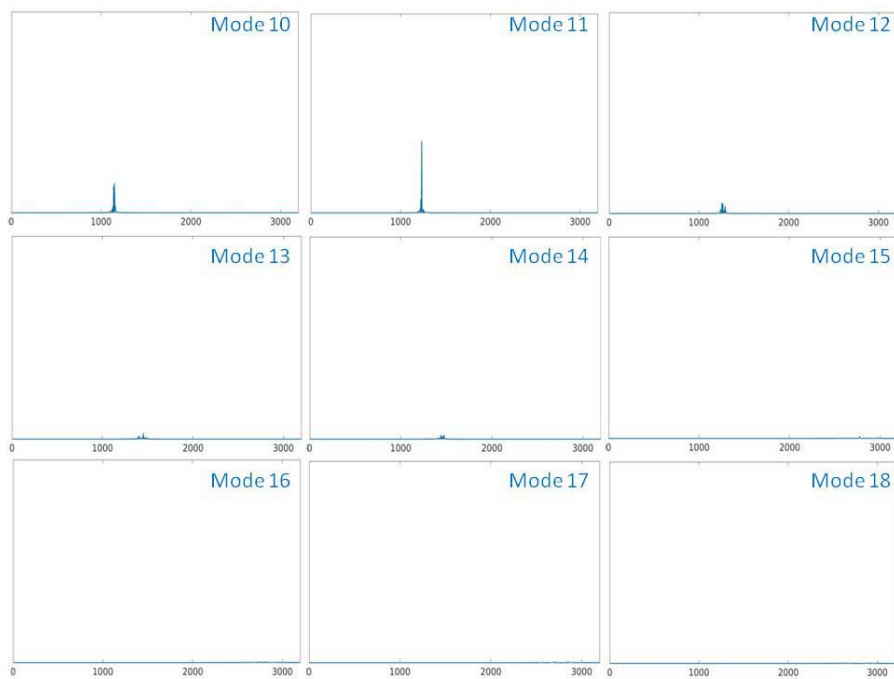
**Figure 8:** Same as Figure 7; different modes.

Each box in these figures is the power spectrum for one normal mode. A power spectrum is representative of the amount of energy present in a vibration of a particular frequency.[39] Thus the power spectrum for each mode should contain peaks for the fundamental frequency for that mode or its overtones. It can be inferred from the spectra that energy is localized in modes 1, 3, 7, 10 and 11. It must be noted that the peak in the spectrum for mode 1 is located at around 200 cm^{-1}, whereas the vibrational frequency for this mode is 111cm^{-1}. It is most likely that this peak represents the first overtone of this mode.

3.4 Coupled Phase Space Model

So far, the focus of this chapter has been presenting data obtained from various calculations. Sections 3.1 and 3.2 highlighted the various trends observed in the *N(t)/N(0)* plots for the trajectory simulations and Section 3.3 attempted to investigate the presence of quasiperiodic trajectories that may be responsible for the extremely small long-time rate constant obtained in the simulations of the random excitation group. Even a cursory look at Table 2 should be enough to notice that among the several groups of trajectory simulations performed, many rate constants seem to be in the range of 0.13-0.21 ps^{-1}. Interestingly, the anharmonic rate constant is 2-3 times larger than these and the occurrence of similar rate constants is all these groups is intriguing to say the least. In this section, an attempt is made to explain the origin of these rate constants and gain a better understanding of the IVR in DO.

A detailed study of energy transfer amongst different modes may be performed by obtaining the power spectrum for various time periods within a trajectory[49]. Although not impossible, such a study is probably not the best approach for studying IVR in molecules with many vibrational degrees of freedom, such as DO. Considering that most reactive molecules have many degrees of freedom, a full dimensional investigation of IVR is difficult. To tackle this problem kinetic models have been developed to gain a qualitative understanding of IVR rates and intrinsic non-RRKM behavior in molecules.[47,48,50] One such model is the two-state coupled phase space model[50] that allows for an investigation into

factors influencing intrinsic non-RRKM nature of a molecule. Extensions of this model, namely the three-state coupled phase space model and two-state-mod model (which allows reaction from both regions) are also available, but will not be considered in this work.
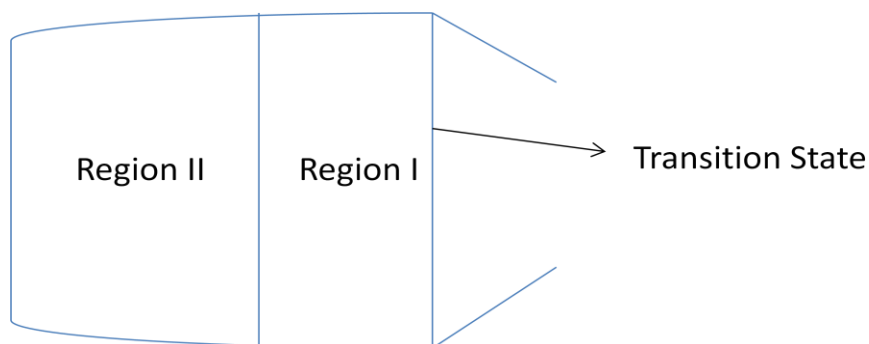
Figure 9: A schematic of the two-state coupled phase space model. Region I is connected to the products via the transition state.

The two-state coupled phase model divides the phase space of the reactant into two regions, regions I and II, which are weakly coupled. Only region I has access to the transition state connecting to the products. Figure 9 shows a schematic of this model. The kinetic scheme is described below.

$$N_1 \xrightarrow{k_1} products \tag{5}$$

$$N_1 \underset{k_3}{\overset{k_2}{\rightleftharpoons}} N_2 \tag{6}$$
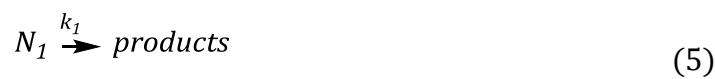
Here, k_1 is the rate constant for product formation from region I, and k_2 and k_3 are the rates for IVR between regions I and II. It can be shown that if a microcanonical ensemble is present at $t = 0$, the RRKM rate constant is:

$$k_0(E) = k_1 k_3 / (k_2 + k_3) \tag{7}$$

At this point, an assumption has been made to apply this model to the system of interest. Vibrational normal modes included in group D (Table 1), which consist of ring

stretch and bend motions, are assumed to constitute region I. All other vibrational modes, i.e. groups A, B and C, make up region II. Thus, this model assumes weak IVR between group D and the other groups.

With this assumption, group D trajectories are such that $N_1(0)=N(0)$ and $N_2(0)=0$. These initial conditions have been used to solve the coupled differential equations that arise from the kinetic schemes *(5)* and *(6)*. The expression thus obtained is:

$$N(t)/N(0) = [(k_1 - \lambda_2)e^{-\lambda_1 t} - (k_1 - \lambda_1)e^{-\lambda_2 t}]/(\lambda_1 - \lambda_2) \tag{8}$$

Here, λ_1 and λ_2 are such that $\lambda_1 + \lambda_2 = k_1 + k_2 + k_3$ and $\lambda_1\lambda_2 = k_1 k_3$. Thus, the two-state coupled phase model predicts a bi-exponential plot for $N(t)/N(0)$ with rate constants λ_1 and λ_2. Values for λ_1, λ_2 and k_1 were obtained by comparing this equation with the bi-exponential fit obtained for group D trajectories in Section 3.1 and used to calculate the values for k_2, k_3 and the RRKM rate constant k_0. Table 3 presents values obtained for all these rate constants.

Table 3: Values for various rate constants obtained from the two-state coupled phase space model.

Rate constant	Value (ps^{-1})
λ_1	3.11
λ_2	0.16
k_1	2.20
k_2	0.85
k_3	0.23
k_0	0.46

Given the assumption that group D modes for DO represent region I, the values obtained for the IVR rate constants between regions I and II are significantly smaller than the rate of formation of products from region I. Moreover, the rate of IVR from region II to region I (k_3) is approximately two times slower than the anharmonic RRKM rate constant.

This is inconsistent with the RRKM assumption that IVR is fast compared to the unimolecular lifetime and hence serves to explain the intrinsic non-RRKM behavior of DO. The RRKM rate constant calculated using the two-state phase space model is $k_o = 0.46$ ps^{-1}, which matches closely with the anharmonic RRKM rate constant of 0.44 ps^{-1} obtained from the random group of trajectories in Section 3.1.

Groups A, B and C are all a part of region II in the two-state coupled phase space model. To obtain a rate constant for such a system where all the molecules are initially present in region II, the steady state approximation[51] can be employed. This approximation is generally used when the rate of formation of an intermediate in a reaction is significantly slower compared to the rate of its dissociation/disappearance. In this case, molecules from region II (N_2) can be treated as the reactants whereas those from region I (N_1) as the intermediate. Since k_1 is almost ten times larger than k_3 the steady state approximation may be employed and the steady state rate constant for the formation of products derived as:

$$k_{ss} = k_1 k_3 / (k_1 + k_2 + k_3) \qquad (9)$$

The value of the steady state rate constant is 0.15 ps^{-1}. It must be noted that k_{ss} is very close to the rate constants obtained for groups A, B and C, which are all in the range of 0.13-0.21 ps^{-1}. The two-state coupled phase space model treats all three groups on an equal footing and cannot distinguish between them, as they are all considered to be a part of region II. Hence, it has implicitly been assumed in this model that the dynamics of all these groups are similar. Despite this assumption, as is evident from the calculations presented here, this model serves excellently to highlight the slow IVR rate constants.

Chapter 4: Conclusion

The primary intent of this work has been to explore and better understand the dynamics of the dissociation of DO using direct dynamics simulations. In spite of the challenges faced in ensuring the reliability of the direct dynamics simulations for a homolytic bond fission system, a simple algorithm was developed to circumvent the instabilities and obtain trajectories that dissociate on the correct PES.

Over the years, unimolecular reactions have been modeled using two distinct approaches: Slater theory and RRKM theory. The former assumes no IVR, whereas the latter assumes complete IVR. It is not very surprising that almost all reactions fall somewhere between these two extremes. The data presented in this work should make it apparent that 1,2-dioxetane is no exception.

Trajectory simulations for excitation groups A, B, C and D shed light on the *apparent* non-RRKM dynamics of the system, where different non-random excitations exhibit varied dissociation dynamics. The trajectory simulations from the random group, serve to label DO as an *intrinsic* non-RRKM molecule. The majority of the dissociation for this simulation group is much slower than the anharmonic RRKM rate constant and the extremely slow long-time rate constant is an indication of quasiperiodic behavior. The existence of quasiperiodic trajectories has been verified by calculating the power spectrum of undissociated trajectories, which further cements DO as an *intrinsic* non-RRKM molecule.

Slow IVR in DO has been modeled using a two-state coupled phase space model, which makes a simple attempt at understanding the bottlenecks in IVR by dividing the phase space into two regions. The use of this model brought to light the slow rate of IVR between group D vibrations and other vibrations, in turn showcasing that the vibrations in the ring are weakly coupled to vibrations outside the ring.

A more detailed study of the vibrational energy transfer between the non-ring modes of the molecule may be possible, but has not been addressed here. The data presented here, especially the similarity between the rates of dissociation arising for group

A, B, C and random and the long-time rate for group D are extremely intriguing and calls for an experimental study into the dissociation dynamics of DO.

References

(1)   O'Neal, H. E.; Richardson, W. H. Thermochemistry of 1,2-Dioxetane and Its
        Methylated Derivatives. Estimate of Activation Parameters. *J. Am. Chem. Soc.* **1970**,
        92 (22), 6553–6557.

(2)   Richardson, W. H.; Hodge, V. F. Neighboring Peroxide Anion and the 1,2-Dioxetane
        Intermediate. Kinetic and Procut Study of the Basic Decomposition of Chloro-Tert-
        Butyl Hydroperoxide. *J. Am. Chem. Soc.* **1971**, *93* (16), 3996–4004.

(3)   Turro, N. J.; Lechtken, P.; Schore, N. E.; Schuster, G.; Steinmetzer, H. C.; Yekta, A.
        Tetramethyl-1,2-Dioxetane. Experiments in Chemiexcitation, Chemiluminescence,
        Photochemistry, Chemical Dynamics, and Spectroscopy. *Acc. Chem. Res.* **1974**, *7* (4),
        97–105.

(4)   Adam, W.; Baader, W. J. Effects of Methylation on the Thermal Stability and
        Chemiluminescence Properties of 1,2-Dioxetanes. *J. Am. Chem. Soc.* **1985**, *107* (2),
        410–416.

(5)   Reguero, M.; Bernardi, F.; Bottoni, A.; Olivucci, M.; Robb, M. A. Chemiluminescent
        Decomposition of 1,2-Dioxetanes: An MC-SCF/MP2 Study with VB Analysis. *J. Am.
        Chem. Soc.* **1991**, *113* (5), 1566–1572.

(6)   Wilsey, S.; Bernardi, F.; Massimo Olivucci; Michael A. Robb; Sean Murphy, and; Adam,
        W. The Thermal Decomposition of 1,2-Dioxetane Revisited. *J. Phys. Chem* **1999**, *103*,
        1669.

(7)   Vico, L. De; Liu, Y.-J.; Krogh, J. W.; Lindh, R. Chemiluminescence of 1,2-Dioxetane.
        Reaction Mechanism Uncovered. *J. Phys. Chem. A* **2007**, *111*, 8013.

(8)   Vacher, M.; Brakestad, A.; Karlsson, H. O.; Fdez. Galván, I.; Lindh, R. Dynamical
        Insights into the Decomposition of 1,2-Dioxetane. *J. Chem. Theory Comput.* **2017**, *13*
        (6), 2448–2457.

(9)   Tanaka, C.; Tanaka, J.; Matsumoto, M. An Intramolecular Charge/electron Transfer

Chemiluminescence Mechanism of Oxidophenyl-Substituted 1,2-Dioxetane. *Phys. Chem. Chem. Phys.* **2011**, *13* (35), 16005.

(10)   Adam, W.; Cilento, G. *Chemical and Biological Generation of Excited States*; Academic Press, 1982.

(11)   Harding, L. B.; Goddard, W. A. Intermediates in the Chemiluminescent Reaction of Singlet Oxygen with Ethylene. Ab Initio Studies. *J. Am. Chem. Soc.* **1977**, *99* (13), 4520–4523.

(12)   Dagaut, P.; Cathonnet, M.; Boettner, J. C. Experimental Study and Kinetic Modeling of Propene Oxidation in a Jet Stirred Flow Reactor. *J. Phys. Chem.* **1988**, *92* (3), 661–671.

(13)   Hua, H.; Ruscic, B.; Wang, B. Theoretical Calculations on the Reaction of Ethylene witsh Oxygen. *Chem. Phys.* **2005**, *311* (3), 335–341.

(14)   Taatjes, C. A. Uncovering the Fundamental Chemistry of Alkyl + O_2 Reactions via Measurements of Product Formation. *J. Phys. Chem. A* **2006**, *110*, 4299.

(15)   Park, K.; West, A.; Raheja, E.; Sellner, B.; Lischka, H.; Windus, T. L.; Hase, W. L. Singlet and Triplet Potential Surfaces for the $O_2+C_2H_4$ Reaction. *J. Chem. Phys.* **2010**, *133* (18), 184306.

(16)   de Jong, W. A.; Lischka, H.; Windus, T. L.; Hase, W. L. Direct Dynamics Simulation of Dioxetane Formation and Decomposition via the Singlet ·O–O–CH_2 –CH_2· Biradical: Non-RRKM Dynamics. *J. Chem. Phys.* **2012**, *137* (4), 44305.

(17)   Paranjothy, M.; Sun, R.; Zhuang, Y.; Hase, W. L. Direct Chemical Dynamics Simulations: Coupling of Classical and Quasiclassical Trajectories with Electronic Structure Theory. *Wiley Interdiscip. Rev. Comput. Mol. Sci.* **2013**, *3* (3), 296–316.

(18)   Baer, T.; Hase, W. L. *Unimolecular Reaction Dynamics : Theory and Experiments*; Oxford University Press, 1996.

(19)   Hase, W. L. Unimolecular and Intramolecular Dynamics. Relationship to Potential

Energy Surface Properties. *J. Phys. Chem.* **1986**, *90* (3), 365–374.

(20)   Uzer, T.; Miller, W. H. Theories of Intramolecular Vibrational Energy Transfer. *Phys. Rep.* **1991**, *199* (2), 73–146.

(21)   Miller, R. E.; Vohralik, P. F.; Watts, R. O. Sub-Doppler Resolution Infrared Spectroscopy of the Acetylene Dimer: A Direct Measurement of the Predissociation Lifetime. *J. Chem. Phys.* **1984**, *80* (11), 5453–5457.

(22)   Johnson, K. E.; Wharton, L.; Levy, D. H. The Photodissociation Lifetime of the van Der Waals Molecule I2He. *J. Chem. Phys.* **1978**, *69* (6), 2719.

(23)   Vande Linde, S. R.; Hase, W. L. Trajectory Studies of S_N2 Nucleophilic Substitution. I. Dynamics of Cl^- $+CH_3Cl$ Reactive Collisions. *J. Chem. Phys.* **1990**, *93* (11), 7962–7980.

(24)   Born, M.; Oppenheimer, R. Zur Quantentheorie Der Molekeln. *Ann. Phys.* **1927**, *389* (20), 457–484.

(25)   Valiev, M.; Bylaska, E. J.; Govind, N.; Kowalski, K.; Straatsma, T. P.; Van Dam, H. J. J.; Wang, D.; Nieplocha, J.; Apra, E.; Windus, T. L.; et al. NWChem: A Comprehensive and Scalable Open-Source Solution for Large Scale Molecular Simulations. *Comput. Phys. Commun.* **2010**, *181* (9), 1477–1489.

(26)   Peslherbe, G. H.; Wang, H.; Hase, W. L. Monte Carlo Sampling for Classical Trajectory Simulations. In *Advances in Chemical Physics*; John Wiley & Sons, Inc., 1999; pp 171–201.

(27)   Hase, W. L.; Buckowski, D. G. Monte Carlo Sampling of a Microcanonical Ensemble of Classical Harmonic Oscillators. *Chem. Phys. Lett.* **1980**, *74* (2), 284–287.

(28)   Hu, X.; Hase, W. L.; Pirraglia, T. Vectorization of the General Monte Carlo Classical Trajectory Program VENUS. *J. Comput. Chem.* **1991**, *12* (8), 1014–1024.

(29)   Lourderaj, U.; Sun, R.; Kohale, S. C.; Barnes, G. L.; de Jong, W. A.; Windus, T. L.; Hase, W. L. The VENUS/NWChem Software Package. Tight Coupling between Chemical

Dynamics Simulations and Electronic Structure Theory. *Comput. Phys. Commun.* **2014**, *185* (3), 1074–1080.

(30) Schlick, T. *Molecular Modeling and Simulation: An Interdisciplinary Guide*; Interdisciplinary Applied Mathematics; Springer New York: New York, NY, 2010; Vol. 21.

(31) Szabo, A.; Ostlund, N. S. *Modern Quantum Chemistry : Introduction to Advanced Electronic Structure Theory*; Dover Publications, 1996.

(32) Jensen, F. *Introduction to Computational Chemistry*; John Wiley & Sons, 2007.

(33) Salem, L.; Rowland, C. The Electronic Properties of Diradicals. *Angew. Chemie Int. Ed. English* **1972**, *11* (2), 92–111.

(34) Bachler, V.; Gottfried Olbrich; Frank Neese, A.; Wieghardt, K. Theoretical Evidence for the Singlet Diradical Character of Square Planar Nickel Complexes Containing Two O-Semiquinonato Type Ligands. *Inorg. Chem.* **2002**, *41*, 4179.

(35) Vaucher, A. C.; Reiher, M. Steering Orbital Optimization out of Local Minima and Saddle Points Toward Lower Energy. *J. Chem. Theory Comput.* **2017**, *13* (3), 1219–1228.

(36) Tóth, Z.; Pulay, P. Finding Symmetry Breaking Hartree-Fock Solutions: The Case of Triplet Instability. *J. Chem. Phys.* **2016**, *145* (16), 164102.

(37) Brickmann, J.; Pfeiffer, R.; Schmidt, P. C. The Transition Between Regular and Chaotic Dynamics and Its Influence on the Vibrational Energy Transfer in Molecules After Local Preparation. *Berichte der Bunsengesellschaft für Phys. Chemie* **1984**, *88* (4), 382–397.

(38) Champeney, D. C. *Fourier Transforms and Their Physical Applications*; Academic Press, 1973.

(39) McDonald, J. D.; Marcus, R. A. Classical Trajectory Study of Internal Energy Distributions in Unimolecular Processes. *J. Chem. Phys.* **1976**, *65* (6), 2180–2192.

(40)   Noid, D. W.; Koszykowski, M. L.; Marcus, R. A. A Spectral Analysis Method of Obtaining Molecular Spectra from Classical Trajectories. *J. Chem. Phys.* **1977**, *67* (2), 404–408.

(41)   Bunker, D. L. Monte Carlo Calculation of Triatomic Dissociation Rates. I. N_2O and O_3. *J. Chem. Phys.* **1962**, *37* (2), 393–403.

(42)   Bhuiyan, L. B.; Hase, W. L. Sum and Density of States for Anharmonic Polyatomic Molecules. Effect of Bend–stretch Coupling. *J. Chem. Phys.* **1983**, *78* (8), 5052–5058.

(43)   Hu, X.; Hase, W. L. Modification of the Duchovic–Hase–Schlegel Potential Energy Function for $H+CH_3 \leftrightarrow CH_4$. Comparison of Canonical Variational Transition State Theory, Trajectory, and Experimental Association Rate Constants. *J. Chem. Phys.* **1991**, *95* (11), 8073–8082.

(44)   Song, K.; Hase, W. L. Fitting Classical Microcanonical Unimolecular Rate Constants to a Modified RRK Expression: Anharmonic and Variational Effects. *J. Chem. Phys.* **1999**, *110* (13), 6198.

(45)   Bunker, D. L.; Hase, W. L. On non-RRKM Unimolecular Kinetics: Molecules in General, and CH_3NC in Particular. *J. Chem. Phys.* **1973**, *59* (9), 4621–4632.

(46)   Noid, D. W.; Koszykowski, M. L.; Marcus, R. A. Quasiperiodic and Stochastic Behavior in Molecules. *Annu. Rev. Phys. Chem.* **1981**, *32* (1), 267–309.

(47)   Lourderaj, U.; Hase, W. L. Theoretical and Computational Studies of Non-RRKM Unimolecular Dynamics. *J. Phys. Chem. A* **2009**, *113* (11), 2236–2253.

(48)   Paranjothy, M.; Sun, R.; Kumar Paul, A.; Hase, W. L. Models for Intrinsic Non-RRKM Dynamics. Decomposition of the SN2 Intermediate $Cl^-–CH_3Br$. *Zeitschrift für Phys. Chemie* **2013**, *227* (9–11), 1361–1379.

(49)   Kato, S. Intramolecular Vibrational Energy Redistribution in $CHCl_3$: A Theoretical Analysis. *J. Chem. Phys.* **1985**, *83* (3), 1085–1094.

(50)   Marcus, R. A.; Hase, W. L.; Swamy, K. RRKM and Non-RRKM Behavior in Chemical

Activation and Related Studies. *J. Phys. Chem.* **1984**, *88* (26), 6717–6720.

(51)   Laidler, K. J. (Keith J. *Chemical Kinetics*; Harper & Row, 1987).